# Supplementary Information for
# Spatiotemporal Imaging of Thickness-Induced Band Bending Junctions

*Joeson Wong[1], Artur Davoyan[1,2], Bolin Liao[3,4], Andrey Krayev[5], Kiyoung Jo[6], Eli Rotenberg[7], Aaron Bostwick[7], Chris M. Jozwiak[7], Deep Jariwala[1,6], Ahmed H. Zewail[3, ǂ], Harry A. Atwater[1, *]*

1. Department of Applied Physics and Materials Science, California Institute of Technology, Pasadena, CA, USA
2. Department of Mechanical and Aerospace Engineering, University of California, Los Angeles, CA, USA
3. Department of Chemistry, California Institute of Technology, Pasadena, CA, USA
4. Department of Mechanical Engineering, University of California, Santa Barbara, CA, USA
5. Horiba Scientific, Novato, CA, USA
6. Department of Electrical and Systems Engineering, University of Pennsylvania, Philadelphia, PA, USA
7. Advanced Light Source, Lawrence Berkeley National Lab, Berkeley, CA, USA

ǂ Deceased

*Corresponding Author: Harry A Atwater (haa@caltech.edu)

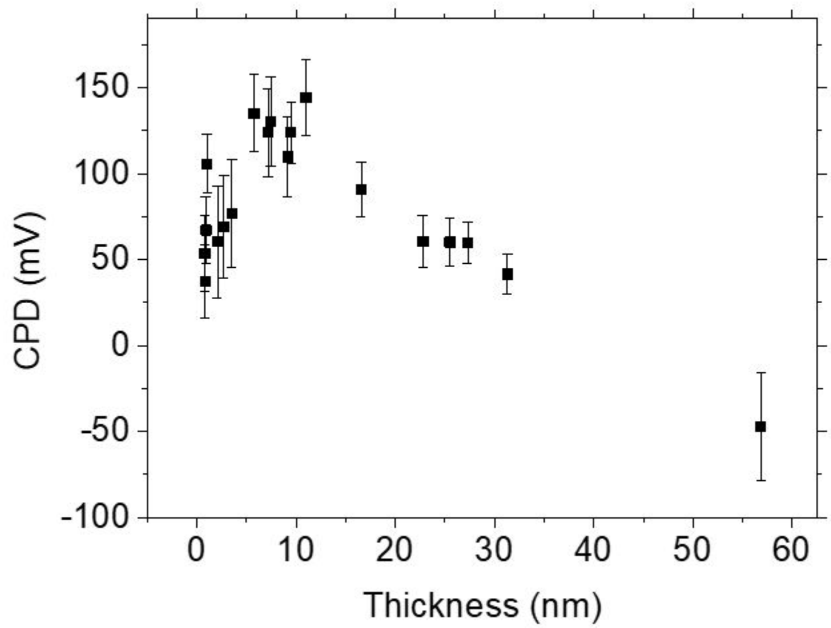


**Figure S1.** Contact potential difference of other $MoS_2$ flakes on Au: Measured contact potential difference of $MoS_2$ on Au for a variety of thicknesses. OmegaScope-R (AIST-NT) setup was used for KPFM with concurrent AFM measurement. Au tip was biased by 3 V and connected to a lock-in amplifier while the sample was grounded. $R_a$ (arithmetic average) values were obtained from a standard sized region of each layer of flakes comprising 300x300 points and the standard deviations in $R_a$ values were plotted as error bars. The lateral areas (sizes) of the flakes ranged from 20-50 $\mu m^2$

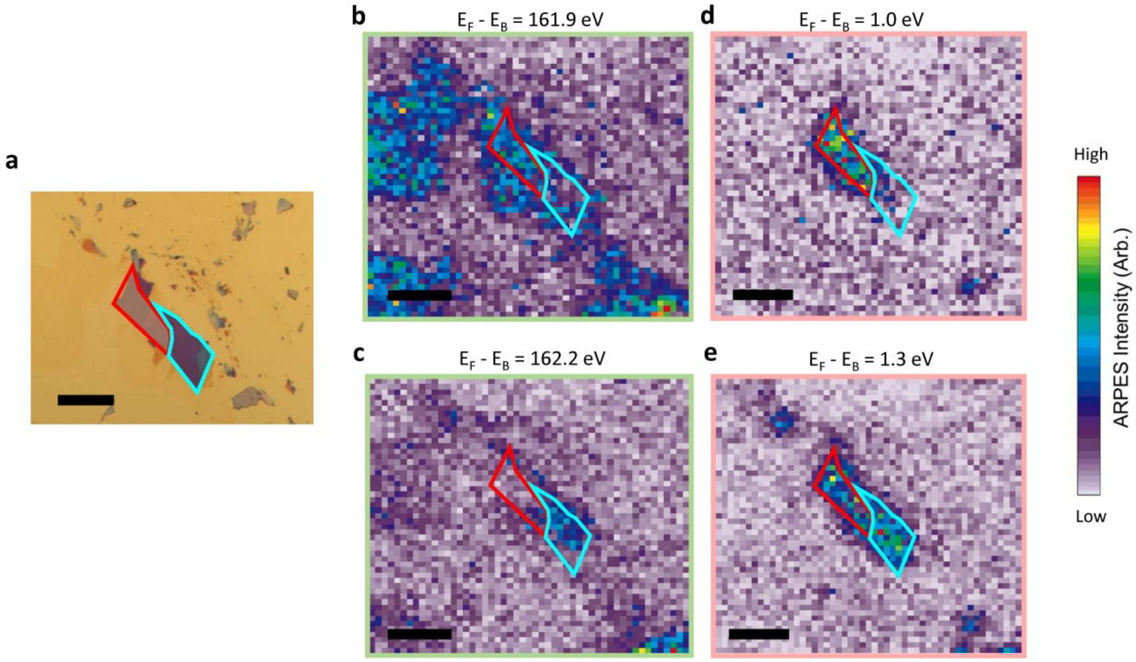


**Figure S2.** Photoemission spectroscopy of another $MoS_2$ flake on Au: **(a)** Optical micrograph image of $MoS_2$ exfoliated onto a gold substrate. Intensity map of photoemitted electrons at the sulfur 2p core level for binding energies of 161.9 eV **(b)** and 162.2 eV **(c)**. Intensity map of photoemitted electrons from the valence band of $MoS_2$ resolved to its Γ point for binding energies of 1.0 eV **(d)** and 1.3 eV **(e)**. All scale bars are 50 $\mu$m. The red and cyan overlays correspond to thick and thin portions of the sample, respectively.

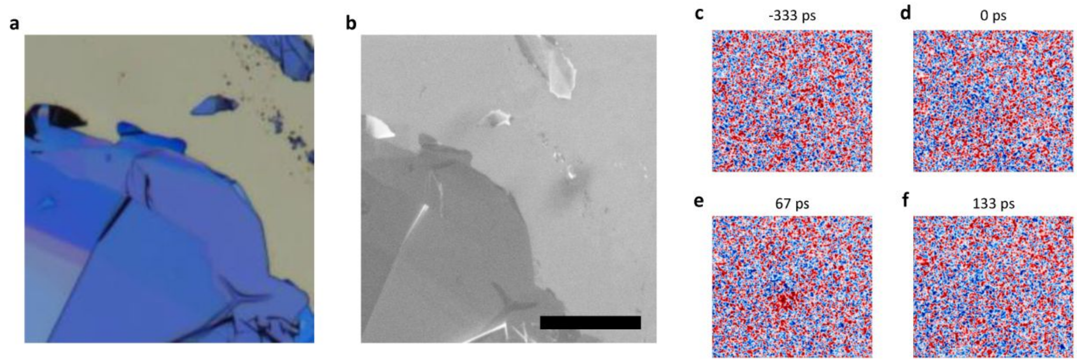


**Figure S3.** Scanning ultrafast electron microscopy of bulk $MoS_2$ on Au: **(a)** Optical micrograph image of a very thick $MoS_2$ exfoliated onto a gold substrate. **(b)** Static SEM image of the same flake (scale bar = 100 $\mu$m). Contrast images formed at different pump-probe time delays of **(c)** -333 ps **(d)** 0 ps **(e)** 67 ps and **(f)** 133 ps, suggesting that vertical carrier separation in very thick $MoS_2$ on Au is unobservable through SUEM because its thickness is much larger than the band-bending Debye screening length. In the contrast images, (c) – (f), the color bar is blue (red) for excess electrons (holes). Contrast images are taken over the same region as the static SEM image in (b).

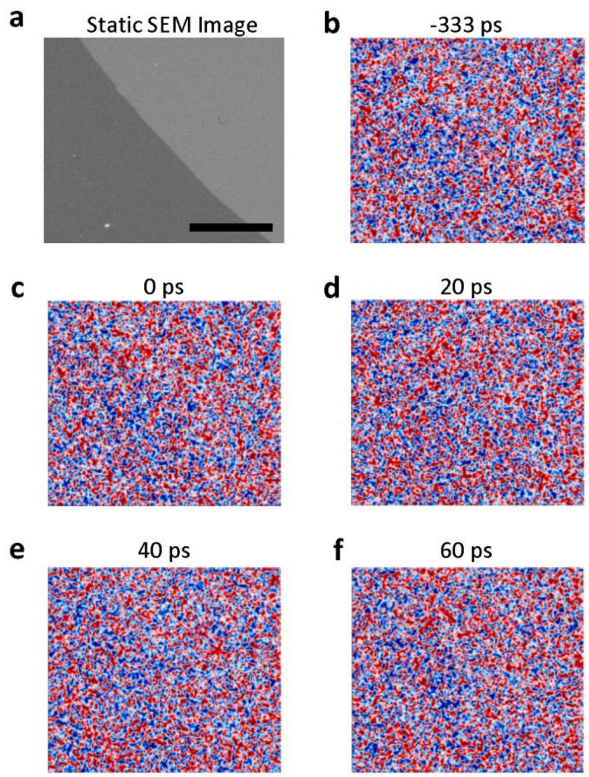


**Figure S4.** Scanning ultrafast electron microscopy of monolayer $MoS_2$ on Au: **(a)** Static SEM image of a monolayer $MoS_2$ on Au (scale bar = 100 $\mu$m). Contrast images formed at different pump-probe time delays of **(b)** -333 ps **(c)** 0 ps **(d)** 20 ps **(e)** 40 ps and **(f)** 60 ps, suggesting that vertical carrier separation in monolayer $MoS_2$ on Au is unobservable through SUEM because its thickness is much smaller than the band-bending Debye screening length. In the contrast images, (b) – (f), the color bar is blue (red) for excess electrons (holes). Contrast images are taken over the same region as the static SEM image in (a).

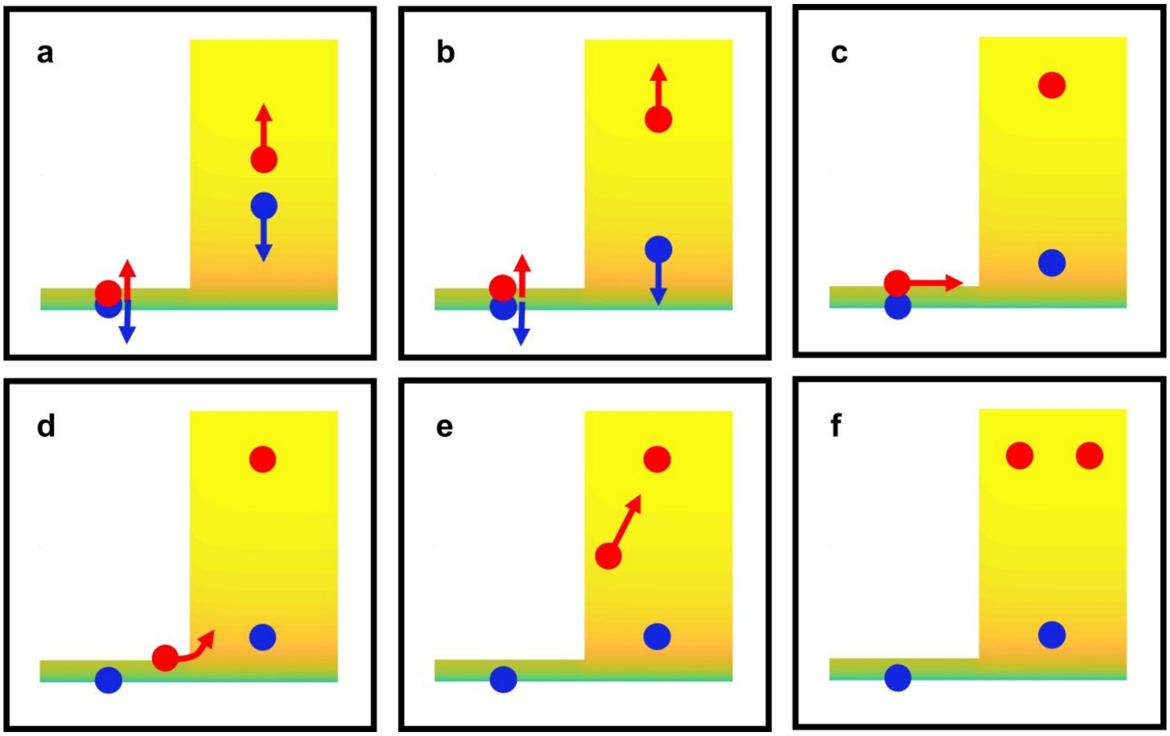


**Figure S5.** Schematic depiction of carrier transport at a band bending junction: In a band bending junction, carriers transport vertically before separating laterally. The population of holes (electrons) are depicted by red (blue) circles. Arrows represent the direction of the flow of carriers. Time is increasing from **(a)** to **(f)**, where **(a)** corresponds to when carriers are first generated and **(f)** corresponds to when carriers have fully separated due to this thickness junction.

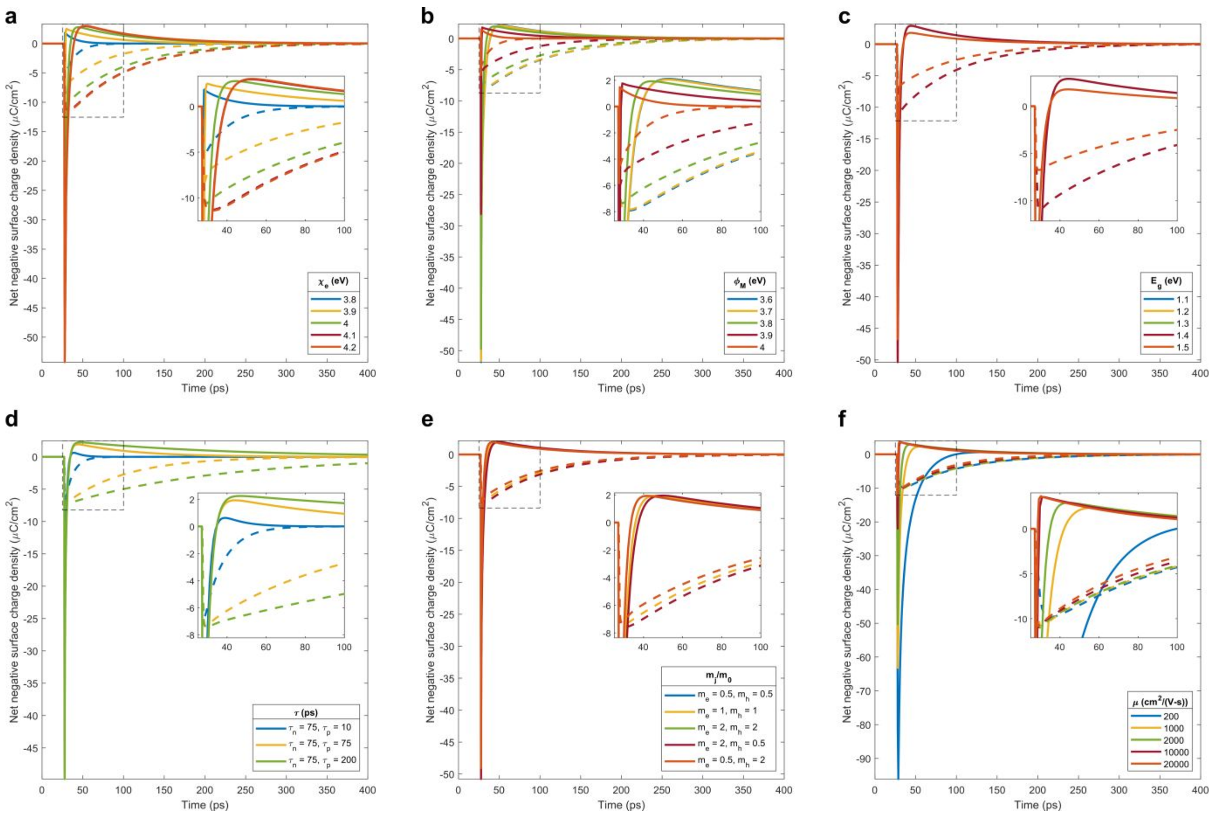


**Figure S6.** Simulated carrier dynamics for various material parameters: Net negative surface charge density of the thin (10 nm, solid line) and thick (100 nm, dashed line) areas of the sample for varying **(a)** electron affinity **(b)** metal workfunction **(c)** bandgap **(d)** carrier lifetime **(e)** effective mass **(f)** and carrier mobility. In all cases, the thin and thick portion of the sample exhibits rapid onset of hole surface charges. The thin portion of the sample then exhibits lateral hole transport to the thick portion of the sample, which results in electrons (holes) separated to the thin (thick) portion of the sample. Dashed lines correspond to the region of the inset. For the bandgap sweep (c), all $E_g < 1.4$ eV overlay with the 1.4 eV curve since the semiconductor is already degenerately doped and there is minimal change to the band profile. Similar effects occur for $\chi_e > 4.1$ eV and $\phi_M < 3.7$ eV. For the effective mass sweep (e), varying the effective mass of the electron does little to the carrier dynamics because the transport is dominated by the minority carrier, i.e., the holes (see also Figure S7).

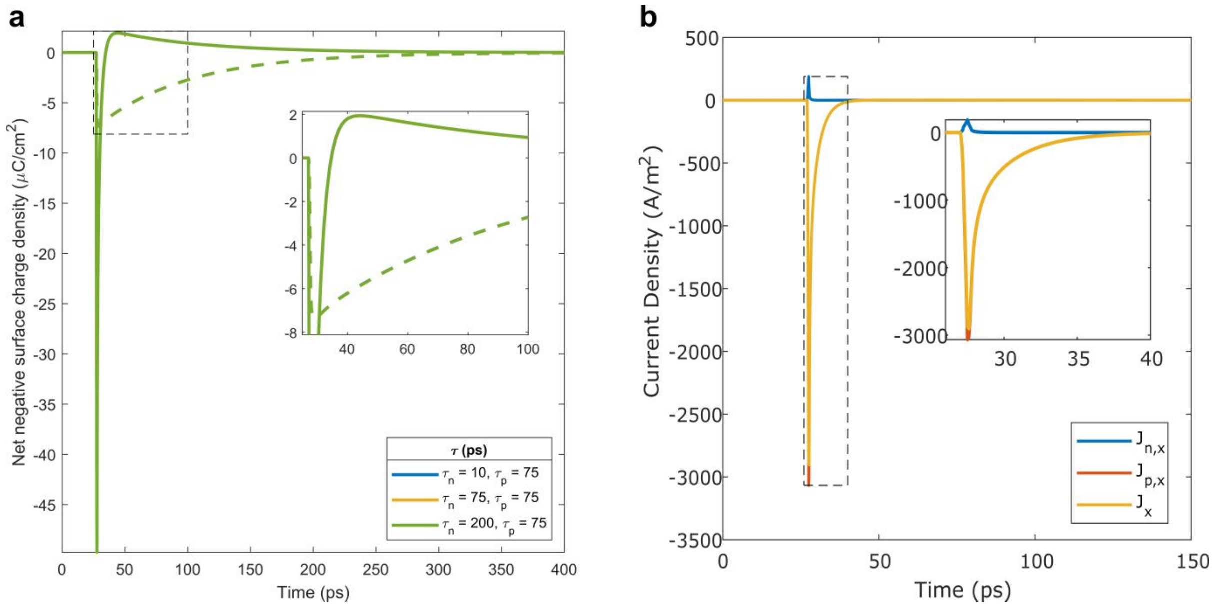


**Figure S7.** Hole dominated charge transport: **(a)** Simulated charge density plots for varying electron lifetime. All curves are overlaid on top of one another, showing that the minority carrier, i.e., the holes, dominate the carrier flow. **(b)** Simulated electron $J_n$, hole $J_p$, and total $J$ current density at the thin-thick junction, showing again that the carrier transport dynamics are dominated by the holes. Current densities are resolved to the $x$ direction, showing only the lateral transport characteristics. Dashed box refers to the inset.